Dear Author,

Here are the proofs of your article.

- You can submit your corrections **online**, via **e-mail** or by **fax**.
- For **online** submission please insert your corrections in the online correction form. Always indicate the line number to which the correction refers.
- You can also insert your corrections in the proof PDF and **email** the annotated PDF.
- For fax submission, please ensure that your corrections are clearly legible. Use a fine black pen and write the correction in the margin, not too close to the edge of the page.
- Remember to note the **journal title**, **article number**, and **your name** when sending your response via e-mail or fax.
- **Check** the metadata sheet to make sure that the header information, especially author names and the corresponding affiliations are correctly shown.
- **Check** the questions that may have arisen during copy editing and insert your answers/ corrections.
- **Check** that the text is complete and that all figures, tables and their legends are included. Also check the accuracy of special characters, equations, and electronic supplementary material if applicable. If necessary refer to the *Edited manuscript*.
- The publication of inaccurate data such as dosages and units can have serious consequences. Please take particular care that all such details are correct.
- Please **do not** make changes that involve only matters of style. We have generally introduced forms that follow the journal's style.
  Substantial changes in content, e.g., new results, corrected values, title and authorship are not allowed without the approval of the responsible editor. In such a case, please contact the Editorial Office and return his/her consent together with the proof.
- If we do not receive your corrections **within 48 hours**, we will send you a reminder.
- Your article will be published **Online First** approximately one week after receipt of your corrected proofs. This is the **official first publication** citable with the DOI. **Further changes are, therefore, not possible.**
- The **printed version** will follow in a forthcoming issue.

Please note

After online publication, subscribers (personal/institutional) to this journal will have access to the complete article via the DOI using the URL: http://dx.doi.org/[DOI].
If you would like to know when your article has been published online, take advantage of our free alert service. For registration and further information go to: http://www.link.springer.com.

Due to the electronic nature of the procedure, the manuscript and the original figures will only be returned to you on special request. When you return your corrections, please inform us if you would like to have these documents returned.

Metadata of the article that will be visualized in OnlineFirst

ArticleTitle	A Hamiltonian Particle Method with a Staggered Particle Technique for Simulating Seismic Wave Propagation	
Article Sub-Title		
Article CopyRight	Springer Basel (This will be the copyright line in the final PDF)	
Journal Name	Pure and Applied Geophysics	

Corresponding Author	Family Name	**Takekawa**
	Particle	
	Given Name	**Junichi**
	Suffix	
	Division	Department of Civil and Earth Resources Engineering
	Organization	Kyoto University
	Address	C1-1-111, Kyotodaigaku-Katsura, Nishikyo-ku, Kyoto, Japan
	Email	takekawa@tansa.kumst.kyoto-u.ac.jp
Author	Family Name	**Mikada**
	Particle	
	Given Name	**Hitoshi**
	Suffix	
	Division	Department of Civil and Earth Resources Engineering
	Organization	Kyoto University
	Address	C1-1-112, Kyotodaigaku-Katsura, Nishikyo-ku, Kyoto, Japan
	Email	mikada@gakushikai.jp
Author	Family Name	**Goto**
	Particle	
	Given Name	**Tada-nori**
	Suffix	
	Division	Department of Civil and Earth Resources Engineering
	Organization	Kyoto University
	Address	C1-1-113, Kyotodaigaku-Katsura, Nishikyo-ku, Kyoto, Japan
	Email	goto.tadanori.8a@kyoto-u.ac.jp

	Received	8 April 2013
Schedule	Revised	15 October 2013
	Accepted	19 December 2013

Abstract

We present a Hamiltonian particle method (HPM) with a staggered particle technique for simulating seismic wave propagation. In the conventional HPM, physical variables, such as particle displacement and stress, are defined at the center, i.e., at the same position, of each particle. As most seismic simulations using finite difference methods (FDM) are practiced with staggered grid techniques, we know the staggered alignment of space variables could improve the numerical accuracy. In the present study, we hypothesized that staggered technique could improve the numerical accuracy also in the HPM and tested the hypothesis. First, we conducted a plane wave analysis for the HPM with the staggered particles in order to verify the validity of our strategy. The comparison of grid dispersion in our strategy with that in the conventional one suggests that the accuracy would be improved dramatically by use of the staggered technique. It is also observed that the dispersion of waves is dependent on the propagation direction due to the difference in the average spacing of the neighboring two particles for the same parameters, as is usually observed in FDM with a rotated staggered

	grid. Next, we compared the results from the conventional Lamb's problem using our HPM with those from an analytical approach in order to demonstrate the effectiveness of the staggered particle technique. Our results showed better agreement with the analytical solutions than those from HPM without the staggered particles. We conclude that the staggered particle technique would be a method to improve the calculation accuracy in the simulation of seismic wave propagation.
Keywords (separated by '-')	Particle method - mesh-free method - computational seismology - seismic wave propagation - Lamb's problem
Footnote Information	

Pure Appl. Geophys.

DOI 10.1007/s00024-013-0763-x

Pure and Applied Geophysics

A Hamiltonian Particle Method with a Staggered Particle Technique for Simulating Seismic Wave Propagation

JUNICHI TAKEKAWA,[1] HITOSHI MIKADA,[2] and TADA-NORI GOTO[3]

Abstract—We present a Hamiltonian particle method (HPM) with a staggered particle technique for simulating seismic wave propagation. In the conventional HPM, physical variables, such as particle displacement and stress, are defined at the center, i.e., at the same position, of each particle. As most seismic simulations using finite difference methods (FDM) are practiced with staggered grid techniques, we know the staggered alignment of space variables could improve the numerical accuracy. In the present study, we hypothesized that staggered technique could improve the numerical accuracy also in the HPM and tested the hypothesis. First, we conducted a plane wave analysis for the HPM with the staggered particles in order to verify the validity of our strategy. The comparison of grid dispersion in our strategy with that in the conventional one suggests that the accuracy would be improved dramatically by use of the staggered technique. It is also observed that the dispersion of waves is dependent on the propagation direction due to the difference in the average spacing of the neighboring two particles for the same parameters, as is usually observed in FDM with a rotated staggered grid. Next, we compared the results from the conventional Lamb's problem using our HPM with those from an analytical approach in order to demonstrate the effectiveness of the staggered particle technique. Our results showed better agreement with the analytical solutions than those from HPM without the staggered particles. We conclude that the staggered particle technique would be a method to improve the calculation accuracy in the simulation of seismic wave propagation.

Key words: Particle method, mesh-free method, computational seismology, seismic wave propagation, Lamb's problem.

[1] Department of Civil and Earth Resources Engineering, Kyoto University, C1-1-111, Kyotodaigaku-Katsura, Nishikyo-ku, Kyoto, Japan. E-mail: takekawa@tansa.kumst.kyoto-u.ac.jp

[2] Department of Civil and Earth Resources Engineering, Kyoto University, C1-1-112, Kyotodaigaku-Katsura, Nishikyo-ku, Kyoto, Japan. E-mail: mikada@gakushikai.jp

[3] Department of Civil and Earth Resources Engineering, Kyoto University, C1-1-113, Kyotodaigaku-Katsura, Nishikyo-ku, Kyoto, Japan. E-mail: goto.tadanori.8a@kyoto-u.ac.jp

1. *Introduction*

Seismic modeling techniques have been used for the predictions of strong ground motion caused by earthquakes (GRAVES 1996; KOMATITSCH and TROMP 1999; KOKETSU 2004; AOCHI 2013; NOGUCHI 2013), investigations in rock physics (SAENGER and SHAPIRO 2002; SAENGER 2011; MADONNA 2012), exploration seismology (GELIS 2005; ZENG 2012), etc. Because of the importance of seismic modeling, many numerical schemes have been developed in order to improve the numerical accuracy or the computational efficiencies.

Among various schemes, the finite difference method (FDM) has been widely used for its accuracy and simplicity in the seismological field. MADARIAGA (1976) first applied a scheme based on staggered grids to solve dynamics of an expanding circular fault. VIRIEUX (1984, 1986) applied a staggered grid technique to simulate seismic wave propagation in order to improve the accuracy of FDM. In FDM with a staggered grid, the velocity and stress components are defined at two different sets of grid points staggered to each other. Later, SAENGER (2000) developed a rotated staggered grid method to calculate seismic wave propagation in arbitrary heterogeneous and anisotropic media. BERNTH and CHAPMAN (2011) analyzed and compared the accuracy and computational requirements of various staggered grid schemes. Since these techniques improve the accuracy without sacrificing the computational costs, many researchers and engineers are using these techniques.

Recently, particle-based methods have also been applied to simulations of seismic wave propagation as an alternative to traditional continuum-based simulators. TOOMEY and BEAN (2000), DELL VALLE-GARCIA

(2003) developed elastic lattice methods (ELM) based on the distinct element method (Cundall and Strack 1979) for the seismic wave simulations. Takekawa *et al.* (2013) applied a moving particle semi-implicit (MPS) method to the coupled simulations of the seismic wave propagation and failure phenomena. In ELM and the MPS method, the particle velocities or the displacements are defined at the centers of the particle positions, whereas the interaction forces are defined at the middle positions between the particles. (Takekawa 2012) applied a Hamiltonian particle method (HPM), originally developed by Suzuki and Koshizuka (2008), to numerical simulation of seismic wave propagation. Their results show the applicability of the HPM to simulate seismic wave propagation in an elastic medium with an arbitrary-shaped free surface. In the original HPM, however, either particle velocity or displacement and stress components for every particle are defined at the center of each particle. Although the alignment of physical parameters at the same locations in models could induce an artificial oscillation which degrades the numerical accuracy, there are not many publications for the discussion of such artifacts in the application of HPM without sacrificing the computational costs. As Kondo (2010) developed a method which introduces an artificial force, and dramatically improves the accuracy of the HPM after a compromise on the additional calculation and memory usage for the artificial force for a problem of oscillation of an elastic body, we await discussions on the accuracy and the numerical efficiency of seismic wave propagation simulation using HPM.

In the present study, we applied a staggered particle technique to the HPM for seismic wave propagation in order to improve the accuracy and the numerical efficiency. In our strategy, we define the displacement and stress components at the different positions similar to the other simulators using the FDM. First, we explain the fundamental theory of HPM with the staggered particle alignment. Then we conduct plane wave analyses in order to confirm the validity of our strategy. Finally, we test our numerical method using homogeneous and inhomogeneous models, and compare the results from the HPM with those from the analytical solutions and another numerical method.

2. Method

In this chapter, we explain the basic theory of the HPM and the staggered particle strategy. Figure 1 shows the arrangement of particles. Black and white circles represent main- and sub-particles. At the main-particles, the strain and stress tensors are defined. On the other hand, the displacement, velocity, and acceleration vectors are defined at the sub-particles. Each particle has an influence domain which defines the interacting particles around the particle. Interactions between particles described below are limited by the influence domain.

In the HPM, the deformation gradient tensor is calculated by minimizing the error function e_i as follows.

$$e_i = \sum_j \left| \boldsymbol{F}_i \boldsymbol{r}_{ij}^0 - \boldsymbol{r}_{ij} \right| \tag{1}$$

where $\boldsymbol{F}$ is the deformation gradient tensor, $\boldsymbol{r}_{ij}^0$ and $\boldsymbol{r}_{ij}$ are the initial and current position of sub-particle j relative to main-particle i, respectively. Subscripts i and j indicate main- and sub-particle, respectively. The summation in Eq. (1) is applied to the surrounding sub-particles inside the influence domain of main-particle i. Minimizing the error function derives the following equation for calculating the deformation gradient tensor.

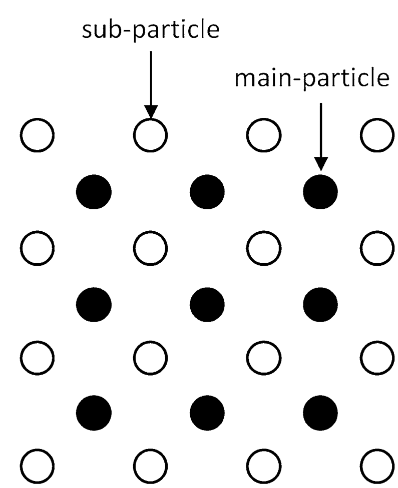

Figure 1
The staggered arrangement of the main- and sub-particles in the present study

$$\boldsymbol{F}_i = \sum_j \boldsymbol{r}_{ij} \otimes \boldsymbol{r}_{ij}^0 \boldsymbol{A}_i^{-1} \tag{2}$$

$$\boldsymbol{A}_i = \sum_j \boldsymbol{r}_{ij}^0 \otimes \boldsymbol{r}_{ij}^0. \tag{3}$$

$\boldsymbol{a} \otimes \boldsymbol{b}$ means tensor product of vector $\boldsymbol{a}$ and $\boldsymbol{b}$. The strain tensor, stress tensor, and the total elastic strain energy can be calculated using the deformation gradient tensor.

$$\boldsymbol{E}_i = \left(\boldsymbol{F}_i^T \boldsymbol{F}_i - \boldsymbol{I}\right)/2 \tag{4}$$

$$\boldsymbol{S}_i = 2\mu \boldsymbol{E}_i + \lambda \mathrm{tr}(\boldsymbol{E}_i)\boldsymbol{I} \tag{5}$$

$$V = \sum_i (\boldsymbol{S}_i : \boldsymbol{E}_i \Delta B_i)/2 \tag{6}$$

where $\boldsymbol{E}$, $\boldsymbol{S}$ and V are the Green–Lagrangian strain tensor, second Piola–Kirchhoff stress tensor and the total elastic strain energy, respectively. ΔB_i is the volume of main-particle i.

Using Hamilton's equations, we can derive the equation of motion for each sub-particle j.

$$\Delta m_j \partial \boldsymbol{v}_j / \partial t = \partial V / \partial \boldsymbol{r}_j = \sum_i \left(\boldsymbol{F}_i \boldsymbol{S}_i \boldsymbol{A}_i^{-1} \boldsymbol{r}_{ji}^0 \Delta B_i \right) \tag{7}$$

where Δm_j is the mass of sub-particle j. The summation in Eq. (7) is also applied to the surrounding main-particles inside the influence domain of sub-particle j. We show an explicit expression of stress and displacement components in Appendix.

3. Dispersion Analysis

We perform a plane wave analysis in order to investigate the dispersion properties of HPM with the staggered particles. Here, we assume that a plane P-wave propagates along the horizontal axis in Fig. 2. The model has a P-wave velocity of $V_P = 3{,}500$ m/s, and a mass density of $\rho = 2{,}200$ kg/m^3. Particle spacing Δx between main particles is 10 m. We consider a plane wave of the form

$$\mathbf{u} = u_0 \exp(-i\omega t + ikx) \tag{8}$$

where k is the wavenumber and ω is the frequency.

We focus on the main-particle "a" in Fig. 2. If the radius of the influence domain is set to the particle spacing, main-particle "a" interacts with sub-particles "1", "6", "7" and "8". Substituting Eq. (8) into Eqs. (2) and (3) yields

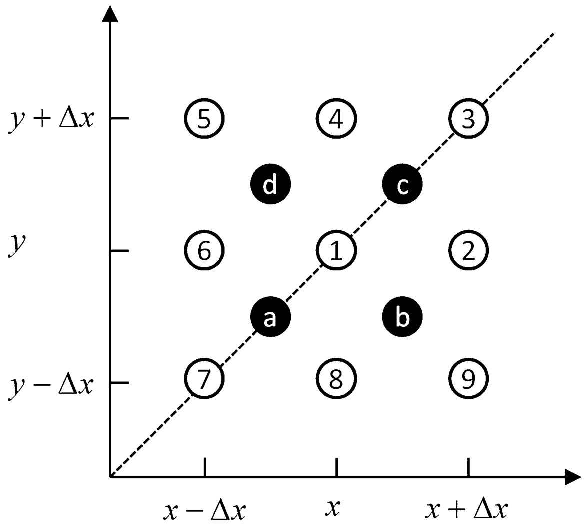

Figure 2
The *numbered* main- and sub-particles for explaining the dispersion analysis

$$\boldsymbol{F}_{\mathrm{a}} = \begin{pmatrix} 1 + (\exp(ik\Delta x) - 1)u_0 \exp(-i\omega t + ikx)/\Delta x & 0 \\ 0 & 1 \end{pmatrix}. \tag{9}$$

Equation (9) is the deformation gradient tensor for the main-particle "a". Inserting Eq. (9) into Eqs. (4) and (5), the stress tensor of the main-particle "a" could be calculated as follows.

$$\boldsymbol{S}_{\mathrm{a}} = \begin{pmatrix} (\lambda + 2\mu)\left\{(1+U)^2 - 1\right\}/2 & 0 \\ 0 & \lambda\left\{(1+U)^2 - 1\right\}/2 \end{pmatrix} \tag{10}$$

where

$$U = (\exp(ik\Delta x) - 1)u_0 \exp(-i\omega t + ikx)/\Delta x. \tag{11}$$

In a similar way, we can calculate the stress tensors for the main-particles "b", "c" and "d". Inserting the deformation gradient tensors and the stress tensors for the main-particles "a", "b", "c" and "d" into the Eq. (7), we can obtain the motion equation for the sub-particle "1" as follows.

$$-\Delta m_1 \omega^2 u_0 \exp(-i\omega t + ikx) = \begin{pmatrix} (\lambda + 2\mu)\{(X - Y)/\Delta x^2 + 3(X^2 - Y^2)/2\Delta x^3 + (X^3 - Y^3)/2\Delta x^4\}\Delta B \\ 0 \end{pmatrix} \quad (12)$$

where

$$\Delta m = \rho \Delta B \quad (13)$$

$$X = (\exp(ik\Delta x) - 1)u_0 \exp(-i\omega t + ikx) \quad (14)$$

$$Y = (1 - \exp(-ik\Delta x))u_0 \exp(-i\omega t + ikx). \quad (15)$$

Here, we assume that the particle spacing is much larger than the amplitude of the incident plane wave. Finally, the relationship between the wavenumber and the frequency can be obtained

$$\omega \approx \sqrt{4(\lambda + 2\mu)/\rho \Delta x^2} \sin(k\Delta x/2). \quad (16)$$

Figure 3a shows the dispersion curve obtained by Eq. (16). For comparison, we also show the dispersion curve for the HPM without the staggered particles (Takekawa 2012). As shown in Fig. 3a, the staggered technique improves the dispersion property dramatically.

Next, we investigate the dependence of the dispersion feature on the wave-propagating direction. We rotate the incident direction of the plane P-wave 45° such that the plane wave propagates along the broken line in Fig. 2. Under the same procedures, we can obtain the dispersion relationship for the inclined incident case as follows

$$\omega \approx \sqrt{2(\lambda + 2\mu)/\rho \Delta x^2} \sin\left(k\Delta x/\sqrt{2}\right). \quad (17)$$

Figure 3b shows the dispersion curves for the case of the different propagating directions. The error for the inclined incidence is larger than that of the horizontal incidence. This feature of the dispersion curve is similar to that of the FDM with the rotated staggered grid (Saenger 2000). This stems from the same relative positions between the points for the displacement and the stress. In any case, our dispersion analysis revealed that the staggered particles improve the accuracy of the HPM without additional calculations like the artificial force.

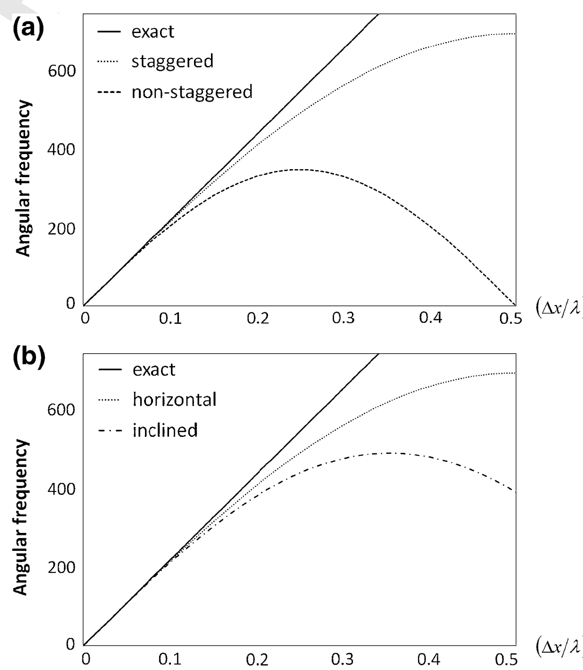

Figure 3
Dispersion curves obtained by the dispersion analyses. **a** Comparison of the result from the HPM with and without the staggered particles. *Dotted* and *broken lines* are the dispersion curves with and without the staggered particles. **b** The dependence of the dispersion curves on the incident directions of the plane wave. *Dotted* and *chain lines* are the dispersion curves of horizontal and inclined incidence, respectively

4. Numerical Examples

In this chapter, we conduct numerical simulations of surface wave propagation using two models in order to demonstrate the effectiveness of our strategy. The first model has a flat free surface without a velocity contrast (i.e. homogeneous model). The second one is a basin model with a strong velocity anomaly around the free surface (i.e. inhomogeneous model). We calculate seismograms with and without the staggered particles for the verification of our strategy. We always use the artificial force (Kondo

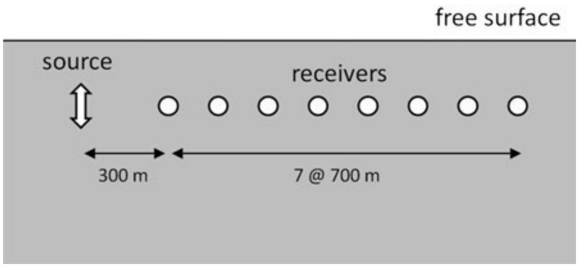

Figure 4
Geometry of the seismic source and receivers in an elastic half-space

2010) stated in the introduction when the staggered particles are not applied (i.e. the original HPM).

4.1. Homogeneous Model

Figure 4 shows our numerical model of a half-space. The seismic source and receivers are located at a depth of 100 m. The source function is a Ricker wavelet with a central frequency of 4 Hz, and the vertical force is applied at the source position. The receivers are set at equal distances from the seismic source, from 300 to 5,200 m. We set the model boundaries well away from the source and receivers in order to avoid the artificial reflection waves instead of applying absorbing boundaries for the surrounding areas.

The spatial and time spacing are set to 10 m and 1 ms, respectively. We studied two models, A and B, of an elastic homogeneous and isotropic medium. The model A has a P-wave velocity of $V_P = 4{,}522$ m/s, an S-wave velocity of $V_S = 1{,}846$ m/s, and a mass density of $\rho = 2{,}200$ kg/m^3. The model B, on the other hand, has a P-wave velocity of $V_P = 2{,}611$ m/s, an S-wave velocity of $V_S = 1{,}846$ m/s, and a mass density of $\rho = 2{,}200$ kg/m^3. Models A and B have Poisson ratios of 0.4 and 0.0, respectively.

We compare our numerical results with the analytical solution of Lamb's problem, and evaluate the misfit by

$$\text{misfit} = \sum_t \left(s^{\text{NUM}}(t) - s^{\text{ANA}}(t)\right)^2 / \sum_t \left(s^{\text{ANA}}(t)\right)^2 \tag{18}$$

where $s^{\text{NUM}}(t)$ and $s^{\text{ANA}}(t)$ are the numerical and analytical seismograms, respectively.

Figure 5 shows the snapshots of the displacement field in the vertical direction calculated by the HPM with the staggered particles after 2 s. In both models, we can observe the P-, S-, and Rayleigh waves. Figure 6 shows the vertical displacement seismograms at each receiver. Solid and dotted lines are analytical and numerical seismograms, respectively. Thick broken lines are the differences between the seismograms amplified by a factor 5. The misfits calculated by Eq. (18) are also shown at the right side of each seismogram. Both seismograms using the staggered particles have good agreement with the analytical ones. At the farthest station, the misfits are <2 and 4 % in models A and B, respectively. On the other hand, the seismograms without the staggered particles have larger errors compared to those with

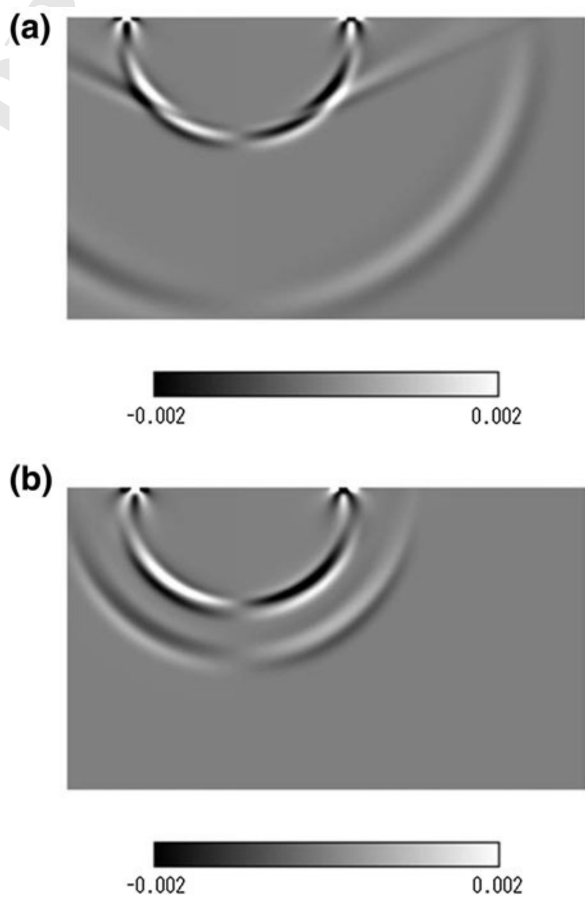

Figure 5
The snapshots of the displacement field in the vertical direction after 2 s for **a** model A, **b** model B using the staggered particles. The contour is measured in meters

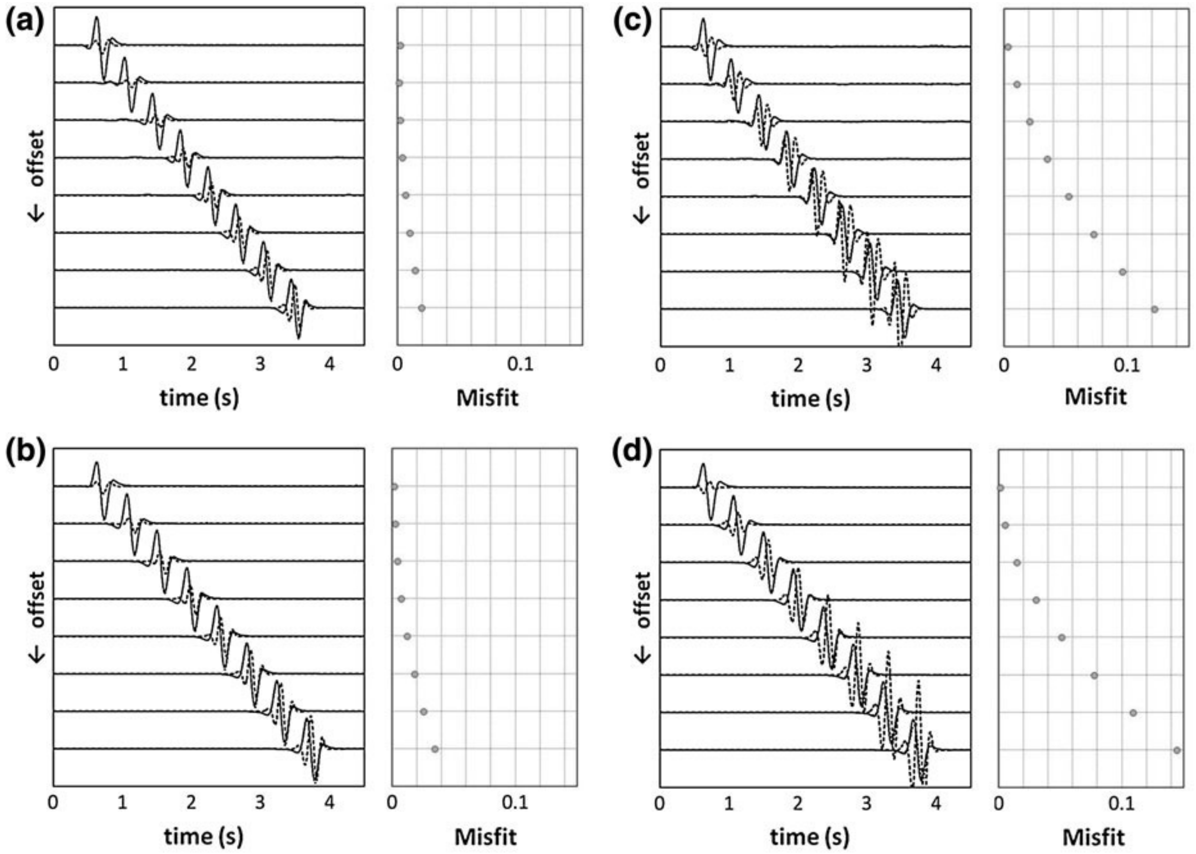

Figure 6
Vertical displacement at the receivers for **a** model A with the staggered particles, **b** model B with the staggered particles, **c** model A without the staggered particles, and **d** model B without the staggered particles. *Solid* and *dotted lines* are the analytical and numerical seismograms, respectively. *Dashed line* is the difference between the seismograms amplified by a factor 5. *Gray circles* on the right side of the seismograms represent the misfits calculated by Eq. (18)

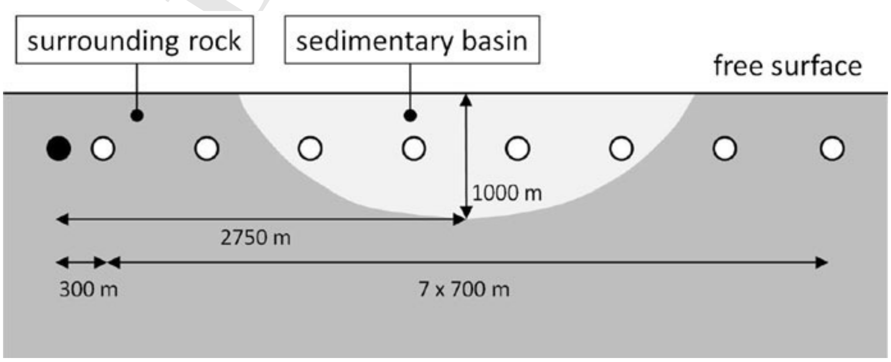

Figure 7
The schematic figure of the inhomogeneous model. A low velocity zone which mimics the sedimentary basin is located at the right side of the seismic source

Journal : Small 24 Dispatch : 16-1-2014 Pages : 11
Article No. : 763 LE TYPESET
MS Code : PAAG-1143 CP DISK

the staggered particles. This means that the staggered particles can improve the accuracy of the simulations of the seismic wave propagation.

Since the maximum modelled frequency in this section is about 11 Hz, the number of particles in a minimum wavelength of model B is about 14. As shown in Fig. 6b, the misfit of the fourth receiver from the seismic source is <1 %. This means that the misfit of our method remains lower than 1 % for a propagation of about 17 wavelengths. The required accuracy depends on individual cases, and the misfit increases with propagation distance due to numerical dispersion as shown in Fig. 6. Therefore, it is difficult to refer to the appropriate number of particles in a wavelength explicitly. The above relationship among the number of particles per wavelength, propagating distance and the observed misfit would be an indication for determining the appropriate particle spacing in individual cases.

4.2. Inhomogeneous Model

Figure 7 shows the schematic figure of the inhomogeneous model. A sedimentary basin, which

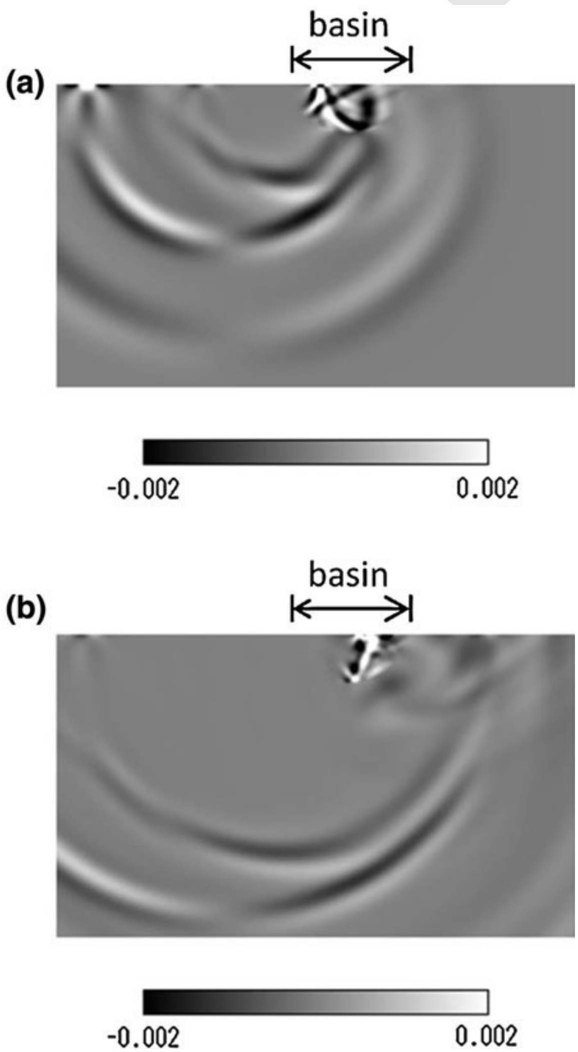

Figure 8
The snapshot of the displacement field in the vertical direction after **a** 2 s, **b** 3 s, respectively. The contour is measured in meters

Journal : Small 24 | Dispatch : 16-1-2014 | Pages : 11
Article No. : 763 | LE | TYPESET
MS Code : PAAG-1143 | CP | DISK

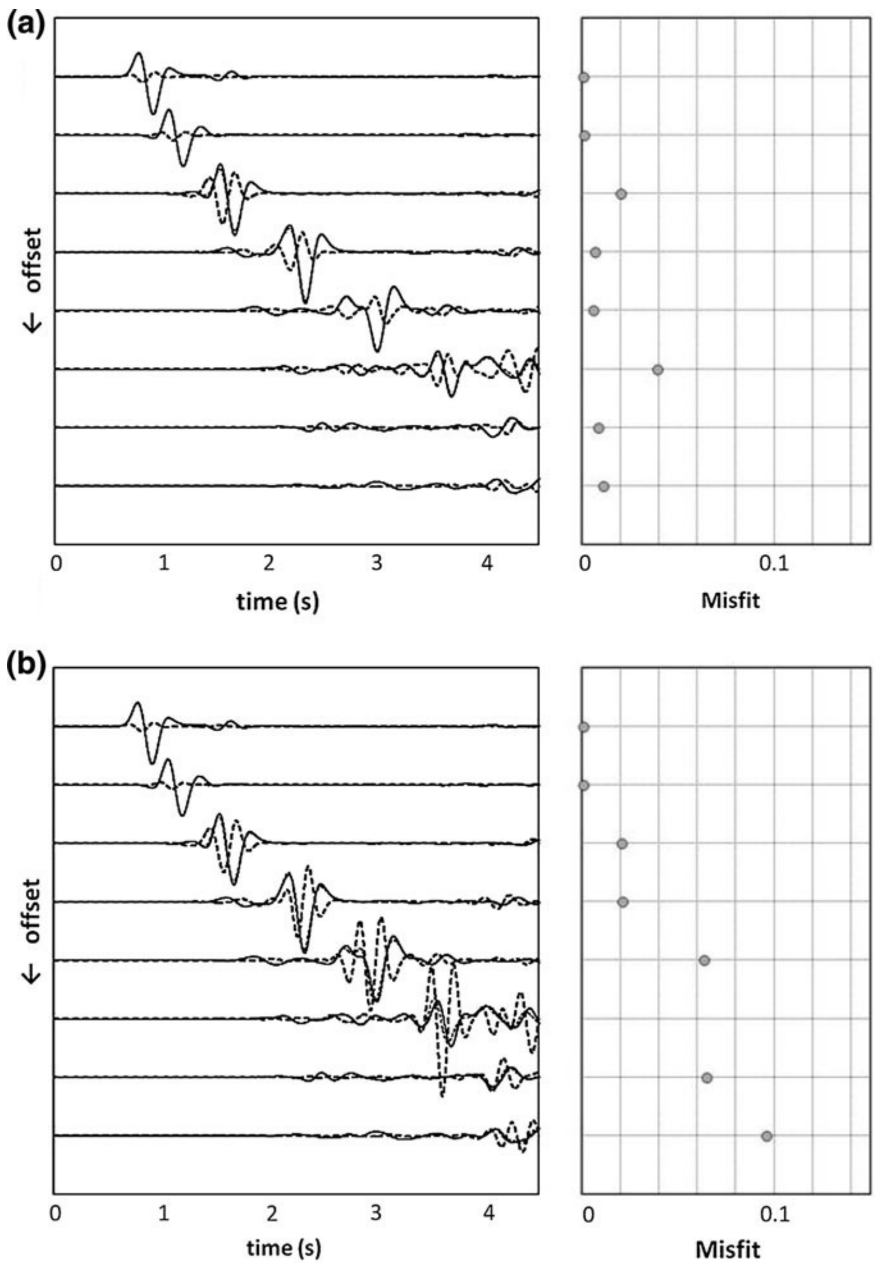

Figure 9
Vertical displacement at the receivers **a** with the staggered particles, and **b** without the staggered particles. *Solid* and *dotted lines* are the FDM-RSG and HPM seismograms, respectively. Other details are the same as in Fig. 6.

has lower velocities compared to the surrounding rock, is located at the right side of the seismic source. The sedimentary basin has a P-wave velocity of $V_P = 2{,}700$ m/s, an S-wave velocity of $V_S = 1{,}102$ m/s, and a mass density of $\rho = 2{,}000$ kg/m^3. The surrounding rock, on the other hand, has a P-wave velocity of $V_P = 4{,}700$ m/s, an S-wave velocity of $V_S = 2{,}878$ m/s, and a mass density of $\rho = 2{,}600$ kg/m^3. The relative positions of the source and receivers are the same as the previous section. The source function is a Ricker wavelet with a central frequency of 3 Hz. Since the calculation of the

Journal : Small 24 Dispatch : 16-1-2014 Pages : 11
Article No. : 763 LE TYPESET
MS Code : PAAG-1143 CP DISK

analytical solution to the arbitrary velocity model is difficult, we use the finite difference method with the rotated staggered grid (FDM-RSG), which allows the method to include strong velocity contrasts without explicitly accounting for them in the numerical method (Saenger 2000), in order to make referential solutions. The grid spacing of the FDM-RSG is twice as fine as that of the HPM for the accurate calculation. The Lame parameters above the free surface are set to zero and the density close to zero for the approximation of a vacuum. This approach can represent the propagation of the surface wave with sufficient accuracy (Bohlen and Saenger 2006). We apply a second-order spatial operator because the application of higher-order operators leads to numerical errors due to the discontinuities of the seismic wave field at the free surface.

Figure 8a, b show the snapshots of the displacement field in the vertical direction calculated by the HPM with the staggered particles after 2 and 3 s, respectively. Trapped waves in the sedimentary basin can be observed. Figure 9 shows the vertical displacement seismograms with and without the staggered particles. The results of the FDM-RSG are also shown in the same figure as solid lines. The waveforms become complex compared to those in the previous section due to the velocity anomaly. The results of the HPM with the staggered particles have better agreement with those of the FDM-RSG than those without the staggered particles. This indicates that the staggered particles can improve the accuracy if the model includes a strong velocity contrast.

5. Conclusions

In the present study, we applied the staggered particle technique to the HPM for simulating seismic wave propagation. We first explained our strategy and conducted the dispersion analyses for investigating the validity of the staggered particles. The results of the dispersion analyses showed the improvement of accuracy by use of the staggered particles. The dependence of the incident direction of the HPM with the staggered particles is similar to that of FDM with a rotated staggered grid. We then conducted surface wave propagation simulations with and without the staggered particles to verify the effectiveness of our strategy using the homogeneous and inhomogeneous models. Numerical waveforms of the HPM with the staggered particles showed better agreement with those from the analytical solutions than those without the staggered particles.

The application of the staggered particles cuts out the need of calculations for the artificial force. This decreases the numerical costs, e.g. calculation time and computational memory. Therefore, our strategy improves not only the accuracy of the HPM, but also the numerical efficiencies.

Acknowledgments

This work was supported by MEXT/JSPS KAKENHI Grant Number 24760361. We thank the editor and anonymous reviewers for their thoughtful comments and suggestions that improved our manuscript.

Appendix

We show an explicit expression of stress and displacement components. We assume that the particle arrangement is shown in Fig. 2 and the distance of each particle in each direction is fixed to Δl. We focus on the main-particle "a" in Fig. 2. The deformation gradient tensor of main-particle "a" is expressed as below.

$$\begin{aligned}
\boldsymbol{F}_{\mathrm{a}} &= \sum_j \boldsymbol{r}_{\mathrm{a}j} \otimes \boldsymbol{r}^0_{\mathrm{a}j} \boldsymbol{A}_{\mathrm{a}}^{-1} = \begin{pmatrix} F_{\mathrm{a}11} & F_{\mathrm{a}12} \\ F_{\mathrm{a}21} & F_{\mathrm{a}22} \end{pmatrix} \\
F_{\mathrm{a}11} &= 1 + \frac{1}{2\Delta l}\left(-u_x^7 + u_x^8 + u_x^1 - u_x^6\right) \\
F_{\mathrm{a}12} &= \frac{1}{2\Delta l}\left(-u_x^7 - u_x^8 + u_x^1 + u_x^6\right) \\
F_{\mathrm{a}21} &= \frac{1}{2\Delta l}\left(-u_y^7 + u_y^8 + u_y^1 - u_y^6\right) \\
F_{\mathrm{a}22} &= 1 + \frac{1}{2\Delta l}\left(-u_y^7 - u_y^8 + u_y^1 + u_y^6\right)
\end{aligned} \tag{19}$$

where u_x^7 represents the displacement of sub-particle "7" in the x-direction. Inserting Eq. (19) into Eq. (4), we obtain the strain tensor for main-particle "a" as follows.

Journal : Small 24 | Dispatch : 16-1-2014 | Pages : 11
Article No. : 763 | LE | TYPESET
MS Code : PAAG-1143 | CP | DISK

$$
\begin{aligned}
\boldsymbol{E}_{\mathrm{a}} &= \frac{1}{2}\left(\boldsymbol{F}_{\mathrm{a}}^{\mathrm{T}}\boldsymbol{F}_{\mathrm{a}} - \boldsymbol{I}\right) = \begin{pmatrix} E_{\mathrm{a}11} & E_{\mathrm{a}12} \\ E_{\mathrm{a}21} & E_{\mathrm{a}22} \end{pmatrix} \\
E_{\mathrm{a}11} &= \frac{1}{2\Delta l}\left(-u_x^7 + u_x^8 + u_x^1 - u_x^6\right) \\
&\quad + \frac{1}{8\Delta l^2}\left\{\left(u_x^{7^2} + u_x^{8^2} + u_x^{1^2} + u_x^{6^2}\right)\right. \\
&\quad \left. +2\left(u_x^7\left(-u_x^8 - u_x^1 + u_x^6\right) + u_x^8\left(u_x^1 - u_x^6\right) - u_x^1 \cdot u_x^6\right)\right\} \\
&\quad + \frac{1}{8\Delta l^2}\left\{\left(u_y^{7^2} + u_y^{8^2} + u_y^{1^2} + u_y^{6^2}\right)\right. \\
&\quad \left. +2\left(u_y^7\left(-u_y^8 - u_y^1 + u_y^6\right) + u_y^8\left(u_y^1 - u_y^6\right) - u_y^1 \cdot u_y^6\right)\right\} \\
E_{\mathrm{a}12} &= \frac{1}{4\Delta l}\left(-u_x^7 - u_x^8 + u_x^1 + u_x^6 - u_y^7 + u_y^8 + u_y^1 - u_y^6\right) \\
&\quad + \frac{1}{8\Delta l^2}\left\{u_x^{7^2} - u_x^{8^2} + u_x^{1^2} - u_x^{6^2}\right. \\
&\quad \left. +2\left(-u_x^7 \cdot u_x^1 + u_x^8 \cdot u_x^6\right)\right\} \\
&\quad + \frac{1}{8\Delta l^2}\left\{u_y^{7^2} - u_y^{8^2} + u_y^{1^2} - u_y^{6^2}\right. \\
&\quad \left. +2\left(-u_y^7 \cdot u_y^1 + u_y^8 \cdot u_y^6\right)\right\} \\
E_{\mathrm{a}12} &= \mathrm{E}_{21} \\
E_{\mathrm{a}22} &= \frac{1}{2\Delta l}\left(-u_y^7 - u_y^8 + u_y^1 + u_y^6\right) \\
&\quad + \frac{1}{8\Delta l^2}\left\{\left(u_x^{7^2} + u_x^{8^2} + u_x^{1^2} + u_x^{6^2}\right)\right. \\
&\quad \left. +2\left(u_x^7\left(u_x^8 - u_x^1 - u_x^6\right) + u_x^8\left(-u_x^1 - u_x^6\right) + u_x^1 \cdot u_x^6\right)\right\} \\
&\quad + \frac{1}{8\Delta l^2}\left\{\left(u_y^{7^2} + u_y^{8^2} + u_y^{1^2} + u_y^{6^2}\right)\right. \\
&\quad \left. +2\left(u_y^7\left(u_y^8 - u_y^1 - u_y^6\right) + u_y^8\left(-u_y^1 - u_y^6\right) + u_y^1 \cdot u_y^6\right)\right\}
\end{aligned} \tag{20}
$$

Inserting Eq. (20) into Eq. (5), the explicit expression for the stress tensor can be obtained

$$
\begin{aligned}
\boldsymbol{S}_{\mathrm{a}} &= 2\mu\boldsymbol{E}_{\mathrm{a}} + \lambda \mathrm{tr}(\boldsymbol{E}_{\mathrm{a}})\boldsymbol{I} = \begin{pmatrix} S_{\mathrm{a}11} & S_{\mathrm{a}12} \\ S_{\mathrm{a}21} & S_{\mathrm{a}22} \end{pmatrix} \\
S_{\mathrm{a}11} &= (\lambda + 2\mu)E_{\mathrm{a}11} + \lambda E_{\mathrm{a}22} \\
S_{\mathrm{a}12} &= 2\mu E_{\mathrm{a}12} \\
S_{\mathrm{a}21} &= 2\mu E_{\mathrm{a}21} \\
S_{\mathrm{a}22} &= (\lambda + 2\mu)E_{\mathrm{a}22} + \lambda E_{\mathrm{a}11}.
\end{aligned} \tag{21}
$$

The same calculations for the other main-particles ("b", "c", "d") are conducted to obtain the deformation gradient and stress tensors. Applying a symplectic scheme to Eq. (7), the following update scheme for the sub-particle "1" can be obtained.

$$
\mathbf{u}_1^{n+1} = \mathbf{u}_1^n + \frac{\Delta t}{\Delta m_1} \cdot \left\{\sum_i \left(\boldsymbol{F}_i \boldsymbol{S}_i \boldsymbol{A}_i^{-1} \boldsymbol{r}_{1i}^0 \Delta B_i\right)\right\}^{n+\frac{1}{2}} \tag{22}
$$

(i = "a", "b", "c", "d"), where the superscript n means the time step. This simple updating scheme is a second-order symplectic integrator which can conserve the total energy with high accuracy.

References

Aochi, H., A. Ducellier, F. Dupros, M. Delatre, T. Ulrich, F. Martin, and M. Yoshimi (2013), *Finite difference simulations of seismic wave propagation for the 2007 Mw 6.6 Niigata-ken Chuetsu-oki earthquake: Validity of models and reliable input ground motion in the near-field*, Pure Appl. Geophys., *170*, 43–64. doi:10.1007/s00024-011-0429-5.

Bernth, H., and C. Chapman (2011), *A comparison of the dispersion relations for anisotropic elastodynamic finite-difference grids*, Geophysics, *76*, WA43–WA50. doi:10.1190/1.3555530.

Bohlen, T., and E. H. Saenger (2006), *Accuracy of heterogeneous staggered-grid finite-difference modeling of Rayleigh waves*, Geophysics, *71*, T109–T115. doi:10.1190/1.2213051.

Cundall, P. A., and O. D. L. Strack (1979), *A discrete numerical model for granular assemblies*, Geotechnique, *29*, 47–65.

Dell Valle-Garcia, R., and F. J. Sanchez-Sesma (2003), *Rayleigh waves modelling using an elastic lattice model*, Geophys. Res. Lett., *30*, 1866.

Gelis, C., D. Leparoux, J. Virieux, A. Bitri, S. Operto, and G. Grandjean (2005), *Numerical modeling of surface waves over shallow cavities*, J. Environ. Eng. Geophys., *10*, 111–121.

Graves, R. W. (1996), *Simulating seismic wave propagation in 3D elastic media using staggered-grid finite differences*, Bull. Seismol. Soc. Am., *86*, 1091–1106.

Koketsu, K., H. Fujiwara, and Y. Ikegami (2004), *Finite-element simulation of seismic ground motion with a voxel mesh*, Pure Appl. Geophys., *161*, 2183–2198.

Komatitsch, D., and J. Tromp (1999), *Introduction to the spectral element method for three-dimensional seismic wave propagation*, Geophys. J. Int., *139*, 806–822.

Kondo, M., Y. Suzuki, and S. Koshizuka (2010), *Suppressing local particle oscillations in the Hamiltonian particle method for elasticity*, Int. J. Numer. Methods Engng., *81*, 1514–1528. doi:10.1002/nme.2744.

Madariaga, R. (1976), *Dynamics of an expanding circular fault*, Bull. Seismol. Soc. Am., *66*, 639–666.

Madonna, C., B. S. G. Almqvist, and E. H. Saenger (2012), *Digital rock physics: numerical prediction of pressure-dependent ultrasonic velocities using micro-CT imaging*, Geophys. J. Int., *189*, 1475–1482. doi:10.1111/j.1365-246X.2012.05437.x.

Noguchi, S., T. Maeda, and T. Furumura (2013), *FDM simulation of an anomalous later phase from the Japan trench subduction zone earthquakes*, Pure Appl. Geophys., *170*, 95–108. doi:10.1007/s00024-011-0412-1.

Saenger, E. H., N. Gold, and S. A. Shapiro (2000), *Modeling the propagation of elastic waves using a modified finite-difference grid*, Wave Motion, *31*, 77–92.

Journal : Small 24 Dispatch : 16-1-2014 Pages : 11
Article No. : 763 ☐ LE ☐ TYPESET
MS Code : PAAG-1143 ☑ CP ☑ DISK

Saenger, E. H., and S. A. Shapiro (2002), *Effective velocities in fractured media: a numerical study using the rotated staggered finite-difference grid*, Geophys. Prospect., *50*, 183–194.

Saenger, E. H., F. Enzmann, Y. Keehm, and H. Steeb (2011), *Digital rock physics: Effect of fluid viscosity on effective elastic properties*, J. Appl. Geophys, *74*, 236–241. doi:10.1016/j.jappgeo.2011.06.001.

Suzuki, Y., and S. Koshizuka (2008), *A Hamiltonian particle method for non-linear elastodynamics*, Int. J. Numer. Methods Engng., *74*, 1344–1373. doi:10.1002/nme.2222.

Takekawa, J., R. Madariaga, H. Mikada, and T. Goto (2012), *Numerical simulation of seismic wave propagation produced by earthquake by using a particle method*, Geophys. J. Int., *191*, 1305–1316. doi 10.1111/j.1365-246X.2012.05676.x.

Takekawa, J., H. Mikada, T. Goto, Y. Sanada, and Y. Ashida (2013), *Coupled simulation of seismic wave propagation and failure phenomena by use of an MPS method*, Pure Appl. Geophys., *170*, 561–570. doi:10.1007/s00024-012-0571-8.

Toomey, A., and C. J. Bean (2000), *Numerical simulation of seismic waves using a discrete particle scheme*, Geophys. J. Int., *141*, 595–604.

Virieux, J. (1984), *SH wave propagation in heterogeneous media: velocity-stress finite-difference method*, Geophysics, *49*, 1933–1957.

Virieux, J. (1986), *P-SV wave propagation in heterogeneous media: velocity-stress finite difference method*, Geophysics, *51*, 889–901.

Zeng, C., J. Xia, R. D. Miller, and G. P. Tsoflias (2012), *An improved vacuum formulation for 2D finite-difference modeling of Rayleigh waves including surface topography and internal discontinuities*, Geophysics, *77*, T1–T9. doi:10.1190/geo2011-0067.1.

(Received April 8, 2013, revised October 15, 2013, accepted December 19, 2013)

	Journal : **Small 24**	Dispatch : **16-1-2014**	Pages : **11**
	Article No. : **763**	☐ LE	☐ TYPESET
	MS Code : **PAAG-1143**	☑ CP	☑ DISK